On the femtosecond laser-induced photochemistry in silver-containing oxide glasses: mechanisms, related optical and physico-chemical properties, and technological applications

Yannick Petit, Sylvain Danto, Théo Guérineau, Alain Abou Khalil, Arthur Le Camus, Evelyne Fargin, Guillaume Duchateau, Jean-Philippe Bérubé, Réal Vallée, Younès Messaddeq, et al.

On the femtosecond laser-induced photochemistry in silver-containing oxide glasses: mechanisms, related optical and physico-chemical properties, and technological applications

Y. Petit, [1, 2, *] *S. Danto,*[1] *T. Guérineau,*[1] *A. Abou Khalil,*[2, 3] *A. Le Camus,*[2, 3] *E. Fargin,*[1] *G. Duchateau,*[2] *J.-P. Bérubé,*[3] *R. Vallée,*[3] *Y. Messaddeq,*[3] *T. Cardinal,*[1] *and L. Canioni*[2]

[1] *University of Bordeaux, CNRS, ICMCB, UMR 5026, 87 avenue du Dr Schweitzer, F-33608 Pessac cedex, France*
[2] *University of Bordeaux, CNRS, CEA, CELIA, UMR 5107, 351 cours de la libération, F-33405 Talence cedex, France*
[3] *Centre d'optique, photonique et laser (COPL), Université Laval, Québec, Canada, G1V 0A6*

[*]Email: yannick.petit@u-bordeaux.fr

Abstract
Laser-induced glass processing has led to huge progress and applications over the last two decades. Here we review recent advances in femtosecond laser-induced photochemistry in isotropic transparent oxide glasses specifically tailored with silver photoactive agents. The understanding of the influence of the considered glass matrix on the nature and properties of the created silver species is of prime importance. After presenting the key material properties, the formation mechanisms of laser-induced silver-based species are discussed, and potential technological applications are highlighted. Laser-induced processing of silver-containing oxide glasses pave the way for the fabrication of complex integrated waveguides and optical circuits with innovative fluorescent, nonlinear optical and plasmonic properties. The universality of the method is expected to extend in any glass materials that show similar laser-induced behavior in terms of silver clusters production.

I. Introduction

Focused femtosecond laser pulses with energies of a few hundreds of nanojoules have become a key tool to modify the physical properties of glass in three dimensions (3D). Because of the nonlinear behavior of the interaction, the energy deposited by a focused femtosecond pulse is confined inside the focal volume, resulting in sub-micrometer spatial resolution for local structuring. Fabrication of 3D integrated photonic structures inside a transparent glass substrate using ultrafast laser inscription is offering unique perspectives for applications in various fields such as astrophotonics [1], optical communication and active devices [2], quantum photonics and emulation of quantum systems [3], optofluidics and sensing [4]. Femtosecond laser-induced photochemistry has been reported in a large variety of glass matrices, including silicates [5, 6], aluminosilicates [7 – 9], aluminoborates [10], but also composite plasmonic metal / dielectric media [11, 12]. The irradiation conditions as well as the intrinsic properties of the material have been optimized to reach the specific and desired response to femtosecond laser exposure. While femtosecond direct laser writing (DLW) has been focusing on the modification of the glass matrix, the introduction of specific centers has been investigated for, for instance, monitoring the photosensitivity of the material or for creating new 3D photonic structures. The role of different ions has been examined such as transition metal ions Cu^{2+} [13], Au^{+} [14], Fe^{3+} and Mn^{3+} [15], and also rare earth ions such as Sm^{3+} [16], Eu^{2+} [17] and Eu^{3+} [18].
Here we will discuss the femtosecond laser-induced photochemistry in silver containing oxide glasses. Among the different ions cited above, the introduction of silver has appeared as the most efficient and fruitful route toward the functionalization of glasses with distinctive properties [19 – 24]. Previous reviews of femtosecond laser-materials interactions have concentrated mainly on commercial materials, such as fused silica, highlighting material modifications such as refractive index changes and void creations [25 – 27]. In this review paper we focus on non-conventional phosphate and gallo-phosphate glass matrices containing silver photosensitive ions and, in the meantime, on the irradiation regime for which photochemical reactions

occur. In fact, the material modifications considered in this review are much weaker than the ones previously reported elsewhere. Indeed, in this regime, photochemistry relies on multiphoton ionization, which provides broad versatility by adapting the order of the absorption nonlinearity to the band gap of the considered material, as far as laser fluences and irradiances remain below optical damage thresholds.
In **Section II**, the glass matrix and its properties are presented. In **Section III**, the mechanisms of energy deposition, structural relaxation and the different photo-ionization processes are introduced. The broad range of physical properties that can be modified is described. Femtosecond lasers can deliver high peak powers while keeping moderate average powers. This particularity makes them perfectly suitable for local interaction and 3D patterning. Finally in **Section IV**, we present promising technological applications with respect to the changes of optical and physico-chemical properties.

II - Glass matrix and silver insertion: silver-sensitized glass materials

The deep understanding of the formation mechanisms of silver clusters or particles in host matrix by femtosecond laser irradiation is essential to achieve on-demand photochemical modifications and new silver species with proper size and shape, inter-particle distances and volume concentration. Considering glasses, the formation mechanism of silver clusters and metallic nanoparticles (NPs) has been widely investigated in soda-lime silica glasses [**28**], oxy-fluoride [**29**], phosphates [**30**].

Direct laser writing using IR femtosecond laser in transparent materials is driven by multiphoton absorption processes. In silver containing phosphate glasses, Bourhis *et al.* [**31**] have demonstrated that, using a 1030 nm femtosecond laser, a four-photon absorption process is responsible for the silver cluster formation. The four-photon wavelength (i.e. 1030/4 = 257 nm) corresponds to the absorption band of the Ag^+ silver ions attributed to the $d^{10} \rightarrow d^9s^1$ transition. Such result indicates that the absorption feature of the silver ions in glass affects the material sensitivity with respect to IR femtosecond laser. The interaction of such glasses with a high repetition rate femtosecond NIR laser leads to the formation of fluorescent silver clusters on the edge of the voxel of interaction. These clusters, composed of less than 10 atoms, result from the reduction of silver ions and the diffusion of silver species from the center to the side of the interaction volume.

Phosphate glass family exhibits many attractive properties. Depending on their composition, they possess good chemical durability, excellent optical properties and ion exchangeability, and fiber drawing ability [**33**, **34**]. They allow for a high rare-earth ions loading with limited clustering effect and thus reduced photo-darkening [**35**]. Such qualities lead to the possibility of fabricating more compact optical gain devices. Furthermore, they have attracted particular attention thanks to their ability to contain relatively large concentration of photosensitive agents such as silver. Depending on the [O]/[P] ratio, phosphate glasses can be made within a broad range of structures, based either on a cross-linked network of Q^3 tetrahedra (vitreous P_2O_5), polymer-like polyphosphate chains of middle-chain Q^2 tetrahedra, 'invert' glasses based on small pyrophosphate units (Q^1) formed of two PO_4 tetrahedral sites or finally on orthophosphate network (with Q^0 units) formed with isolated PO_4 units [**36**] (Fig. 1). Such diversity of glass network structure offers a great variety of material properties.
Among the different phosphate compositions, special attention has been paid recently to zinc-phosphate glasses [**31, 37 – 40**]. In such phosphate glasses, the addition of Al_2O_3 or Ga_2O_3 significantly improves the chemical durability of these glass networks, especially with respect to water etching and solubility. However, such an addition of Al_2O_3 or Ga_2O_3 may also affect the thermodynamics of silver elements, by possibly accelerating the silver cluster clustering and even silver plasmonic nanoparticles formation in zinc phosphate glasses [**41**, **42**].

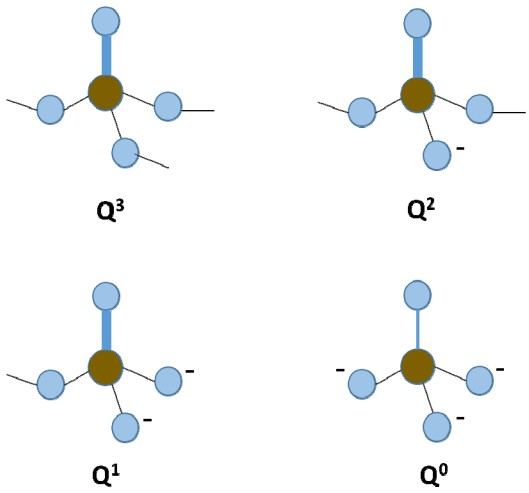

Figure 1. Phosphate tetrahedral PO_4 sites in phosphate glasses: Q^3 cross linking, Q^2 middle chain unit, Q^1 terminal unit, Q^0 isolated unit.

The absorption features of silver ions in glass are directly related to the silver ions distribution, as well as their local environment. The solubility of silver ions in glass is strongly related to the glass matrix composition. In most of silicate, using standard melting techniques, little amount of silver can be introduced. Ionic exchange techniques have been widely developed in order to reach the molar percent range [43], femtosecond direct writing and silver photochemistry become then possible on these glass surfaces. Alternatively, phosphate glasses allow for high silver ions loading, and thanks to this property, multiple achievements have been realized in these materials over the last ten years.

The solubility of the silver ions in the amorphous matrix is a key issue for efficient laser writing. Indeed the silver ions can occupy different sites in the glass matrix, which depends on the glass composition, the material processing and its thermal history. Moreover, energy deposition during femtosecond laser irradiation results from a nonlinear multi-photon absorption process, which is affected by the linear absorption behavior of the glass, especially in the UV cut-off region of the glass [31]. Yet little attention has been paid to the absorption feature in silver containing phosphate glasses and its impact on the overall glass photosensitivity to femtosecond IR laser exposure. The silver ion environment in oxide glass matrices influences both the absorption feature in the UV and the luminescence property of the pristine glass. These properties can be also exploited to investigate the nature of occupied silver sites in the glass matrix.

Various silver ions emission centers have been identified in silver-containing phosphate glasses. An emission attributed to isolated Ag^+ ions coordinated by 6 to 8 oxygen atoms for low silver concentrations was observed in the 300-450 nm spectral domain with fluorescence emission maxima ranging from 325-380 nm in $Na_2O - K_2O - Al_2O_3 - P_2O_5 - Ag_2O$ glasses [44] and in $Na_{1-x}Ag_xPO_3$ and $Na_{1-x}Ag_xZnPO_3$ polyphosphate compositions [45, 46]. The presence of several host sites for Ag^+ ions with close point symmetries was assumed. In the same work a second emission, observed between 450 nm and 750 nm, with a maximum near 550 nm for high concentrations of silver, was associated to the presence of Ag^+--Ag^+ pairs in analogy with the emission in crystalline structure $AgPO_3$. Its intensity increases with the silver content. Similar results were obtained in silver-exchanged silicate glasses [47] and in crystalline and vitreous $AgBaP_3O_9$ polyphosphates [48, 49]. In SrB_4O_7 borates [50], the luminescence of the site emitting at 290 nm was attributed to a crystallographic site of lower symmetry than the one observed in alkali halides. In the specific case of silver-containing zinc phosphate glass matrix ($58ZnO\text{-}42P_2O_5$), the luminescence properties attributed to Ag^+ ions have been investigated [46, 41, 51]. The luminescence spectra for a set of composition (1-x) (55.4 ZnO + 40.3 P_2O_5 + 4.3 Ga_2O_3) + x Ag_2O (oxide molar %) are reported in Fig. 2. For excitation wavelengths inferior to 270 nm, the glasses exhibit a broad emission in the 250-450 nm range (Figs. 2a and 2b). For λ_{exc} = 230 nm, two emission bands can be distinguished with maxima centered at 290 nm and 370 nm (Fig. 2b). With increasing Ag^+ concentration, the relative intensity of the 290 nm band vanishes as compared to the emission at 370 nm. The relative intensities of the two emission bands strongly depend on

the excitation wavelength, as depicted in Fig. 2.When the excitation wavelength is raised up to 280 nm typically, the emission band near 370 nm is favored which indicates the presence of different emitting centers (Fig. 2d).

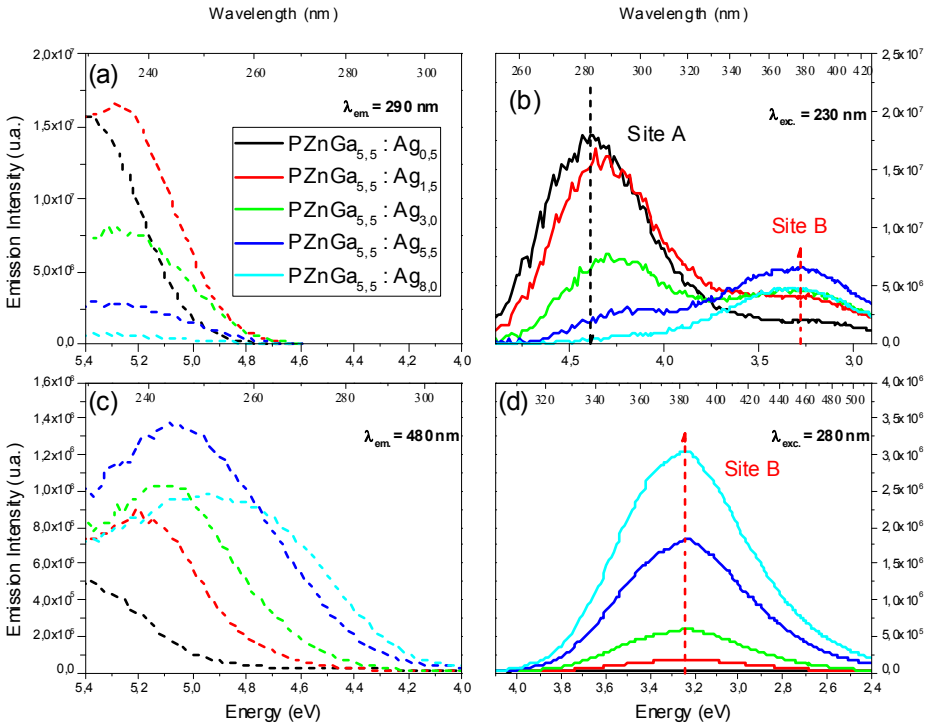

Figure 2. Photo-luminescent properties of silver containing zinc phosphate glasses (1-x) (55.4 ZnO + 40.3 P_2O_5 + 4.3 Ga_2O_3) + x Ag_2O as a function of Ag_2O (oxide molar percent) and evolution of the intensity of the site A versus site B: (a) Excitation graphs for λ_{em} = 290 nm and (b) Emission graphs for λ_{exc} = 230 nm; (c) Excitation graphs for λ_{em} = 480 nm and (d) Emission graphs for λ_{exc} = 280 nm.

Time-resolved luminescence allows for identifying two different lifetimes in accordance with the presence of two emitting centers. For λ_{exc} = 230 nm and λ_{em} = 290 nm, the decay of luminescence lifetime corresponds to a lifetime of 14±2 µs, while for λ_{exc} = 260 nm and λ_{em} = 365 nm, the associated lifetime is about 35±5 µs. The measured decays and the luminescence lifetimes are in accordance with results obtained in silver-containing borates [**50**] and phosphates [**51**]. The emission band appearing at higher wavelength (365 nm) is dominant for the high concentration of silver ions (>3mol% Ag_2O), suggesting a pairing of the silver ions in the glass matrix as proposed by Belharouak *et al.* [**49**]. Similar phenomena have been observed in the system Ga_2O_3 – Na_2O – P_2O_5 [**52**]. Such formation of silver ion pairs, with absorption in the near UV range, has also been reported in different compounds such as halide and phosphate crystals or glass [**48**, **53**].

One has to notice also that depending on the glass matrix structure, namely polyphosphate, pyrophosphate or orthophosphate glasses, the absorption band edge is shifted due to the evolution of the ratio between isolated silver and pairs. For similar silver content, glass network favoring silver pairing such as pyrophosphate clearly exhibit a red-shifted absorption feature, as depicted in Fig. 3 (left). The shift linked directly to the existence of silver ions pairing that concomitantly lead to a red-shifted luminescence excitation band, as compared to the one of isolated silver ions (Fig. 3 (right)).

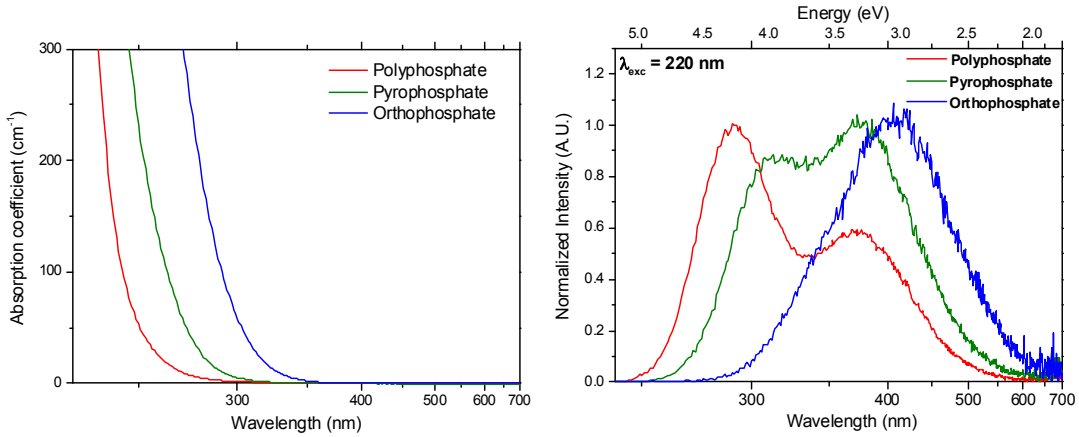

Figure 3. (left) Absorption and (right) emission for excitation at 220 nm for the three glass compositions (expressed in mol%) 61.14 P_2O_5 – 21.58 Ga_2O_3 15.28 Na_2O –2 Ag_2O (poly-phosphate), 46.6 P_2O_5 – 16.45 Ga_2O_3 – 34.95 Na_2O – 2 Ag_2O (pyro-phosphate), 51.53 P_2O_5 – 12.12 Ga_2O_3 – 51.53 Na_2O – 2 Ag_2O (ortho-ophosphate), keeping the ratio Ga_2O_3/P_2O_5=0.35 constant.

The Fig. 4 (a) presents an image of coil fluorescent patterns obtained by DLW for various sample motion speeds on the same polyphosphate, pyrophosphate or orthophosphate glasses than presented in Fig. 3. The Fig 4 (b) shows the corresponding integrated intensity for each pattern. A direct correlation can be established between the presence of silver pairing and the photosensitivity. The ortho-phosphate glass composition, having the largest amount of silver pairing, exhibits the highest photosensitivity toward femtosecond laser writing (Fig 4 (b)). One can propose that the four-photon absorption process is favored thanks to the presence of silver pairing absorbing between 250 and 280 nm [**31**]. This effect demonstrates that both the concentration of silver and the glass matrix structure are of importance for generating silver pairs and thus for tailoring the material photosensitivity. Luminescence spectra of the photo-induced patterns is presented in Fig. 4 (c) for the different glasses while keeping the same DLW laser parameters (Laser irradiance : 16.3 $TW.cm^{-2}$; sample motion speed : 25 $\mu m.s^{-1}$).

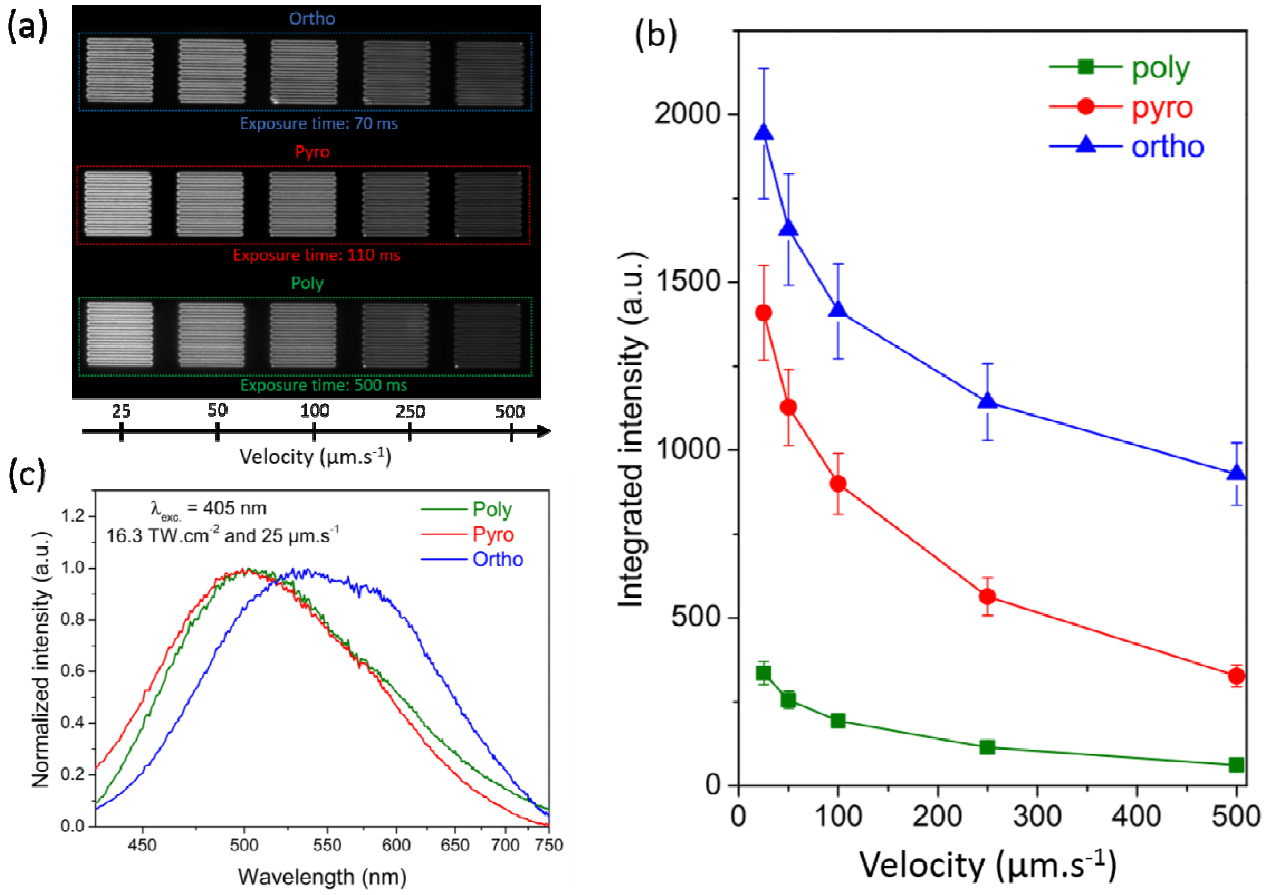

Figure 4. (a) Fluorescence imaging with wide-field excitation at 365 nm of 100x100µm²-dimension fluorescent coil structure obtained with KGW:Yb femtosecond oscillator (up to 2.6 W, 9.1 MHz, 390 femtosecond FWHM at 1030 nm) for 16.3 TW.cm^{-2}-irradiance and various sample motion velocities (25, 50, 100, 250 and 500 µm.s^{-1}) in three relevant glass compositions corresponding to poly-phosphate, pyro-phosphate and ortho-phosphate glasses. Note that imaging exposure time has been adapted for each phosphate glass to avoid any under and overexposure (b) Integrated intensity of the fluorescence imaging of a coil structure for poly-, pyro- and ortho-phosphate glasses for various velocities (25, 50, 100, 250 and 500 µm.s^{-1}) (c) Emission spectra for excitation wavelength at λ_{exc} = 405 nm of the femtosecond laser irradiated area for poly-, pyro- and ortho-phosphate glasses corresponding to DLW parameters : 16.3 TW.cm^{-2} at 25 µm.s^{-1}.

The spectroscopy of laser-induced silver clusters has been investigated in detail, especially in the silver-containing system ZnO - P_2O_5 - Ga_2O_3, with silver oxide molar concentrations corresponding to those of Fig. 2. Laser-induced silver clusters show additional absorption bands that correspond to their fluorescence excitation bands [32]. Such new absorption bands are broad and partially depend on laser irradiation parameters and on the considered silver oxide concentration: the smallest silver cluster species, namely Ag_2^+, showed a band centered at 302 nm (FWHM 34 nm), while larger clusters led to bands centered at 287 nm (FWHM 35) and 340 nm (FWHM 56) [30]. Fluorescence emission of the silver clusters also correspond to a broadband emission that covers the whole visible range and depend on laser irradiation parameters and on the considered composition, showing distinct emission bands with multiple fluorescence decay lifetime in the sub-ns and ns range [30 – 32, 37].

III - Femtosecond laser interaction in silver-containing glasses: mechanisms & properties

III-1. Laser/matter interaction: general mechanisms

Material modification regimes

Femtosecond laser materials interaction has been extensively studied during the past two decades [54 – 58]. The understanding of the involved physical processes and of their associated characteristic times represents a highly complex task since such laser/matter interactions differ with the considered material under investigation and with the irradiation regime. Nevertheless, some elementary processes involved in laser/matter interactions are commonly admitted (Fig. 5). First step deals with energy deposition in the material, corresponding to the partial absorption of the incident laser and the associated generation of photoelectrons. Once thermalized, these electrons then transfer their kinetic energy to the lattice, leading to a well-established local thermodynamical equilibrium. Finally, heat diffusion occurs so as to homogenize the temperature distribution, which can be accompanied by the local melting of the material and its subsequent re-solidification. Globally, this leads to density material modifications labeled as Type 1 regime. In the case of excessive energy deposition, Coulomb explosion can also occur, leading to the creation of voids which is labeled as the Type 3 regime. These two regimes can be accessed with a single pulse, implying that the induced temperature increase is not critical to the resulting modifications [59, 60]. An alternative regime is the Type 2 regime, for which it seems that several pulses incident within a short period of time (µs) are necessary for pulse-after-pulse memory effects to take place during the interaction time [52 – 61]. Finally, softer material modifications can result from laser-induced photochemical reactions, for which the control of the pulse-after-pulse accumulated heat (through the multiple-pulse irradiation at high repetition rates) is even more important. Indeed, in such photochemical regime, heat distribution and diffusion drive both the thermal activation of the chemical species mobility and diffusion inside the temperature gradient, enhancing the photochemical reactivity towards the creation of new species [20, 21, 24, 30, 39, 52 – 67]. The description of such photochemical aspects is a key point of the present review article.

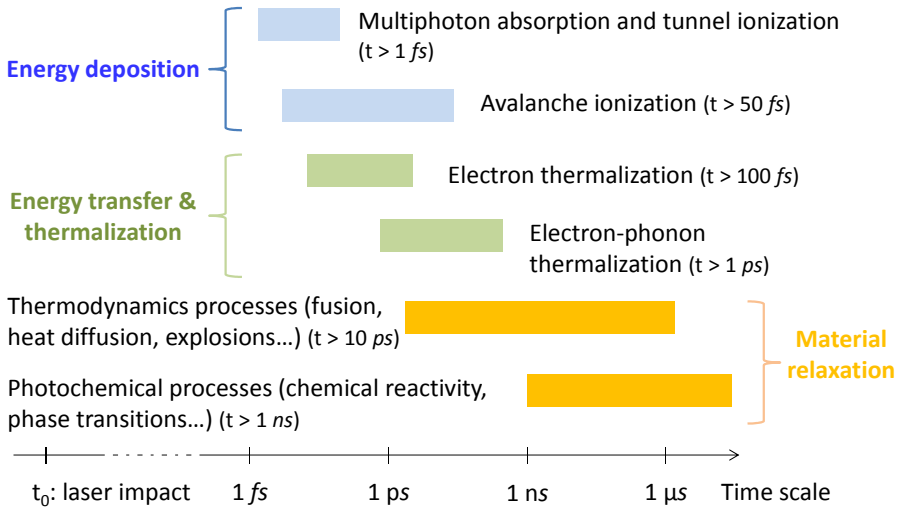

Figure 5. Timescales of the physical phenomena involved in laser-material interaction.

Single-pulse energy deposition

Femtosecond laser energy deposition typically leads to a three-step dynamics, including the creation of free electrons through photo-ionization, their acceleration with additional absorption from the laser field, and finally, additional release of free electrons through avalanche ionization when the kinetic energy of free carriers exceeds the material band gap energy. Multiphoton ionization and tunneling ionization have been theoretically described by Keldysh since 1965 [68]. Multiphoton ionization corresponds to the simultaneous absorption of several photons allowing for a net involved energy to exceed the ionization potential of the electron energy level. Tunneling ionization takes place when the incident electric field is sufficiently high to distort the potential barrier that maintains the electron in the field of the nucleus of an atom. The electron is then ejected by the tunneling effect through the lowered potential barrier. The balance between multiphoton and tunneling ionizations is commonly quantified by the Keldysh parameter $\gamma = \sqrt{m_e c \varepsilon_0 n_0 E_g \omega_L^2 / e^2 I}$, which

implies the ratio between the electron ionization energy and the ponderomotive energy, and where ω_L is the laser angular frequency, m_e and e the mass and the charge of the electron, respectively, c the speed of light in vacuum, n_0 and E_g the refractive index and the band gap energy of the material, respectively, ε_0 the dielectric permittivity of vacuum and I the irradiance [68]. Multiphoton ionization dominates when $\gamma>1$ (*i.e.* for relatively low irradiances). Subsequent avalanche ionization occurs when free electrons are sufficiently accelerated by the laser field to get enough kinetic energy to ionize a neighboring atom by collision. Typical avalanche ionization timescale is 30-50 femtosecond, requiring thus pulse durations longer than such timescale [58, 69]. For shorter pulses, multiphoton "forest fires" ionization has been proposed for intermediate values of the Keldysh parameter ($\gamma\geq1$) with the avalanche-like creation of holes in clusters or molecules [69, 70].

The combined phenomenology of these processes is rather complicated. The interplay between various microscopic physical and chemical mechanisms, associated to different time scales, gives rise to the emergence of a mesoscopic behavior taking place at sub-micrometer spatial scales, ultimately leading to a silver cluster organization in the irradiated material when considering silver-containing glasses, as detailed hereafter.

III-2. Single-pulse interaction and specific laser-induced mechanisms

The general mechanisms presented in **Section III-1** need to be detailed to take into account the multi-physics and multi-scale phenomena that occur in silver-containing glasses during femtosecond laser structuring with high repetition rates. During laser pulse, free electrons are promoted based on multi-photon absorption either from the silver ions Ag^+ or from the phosphate chains of the glass matrix. Such bunch of free electrons leads to the Ag^0-formation kinetic reaction ($Ag^+ + e^- \rightarrow Ag^0$) accordingly to the dependence of the kinetic reaction rate on the components' concentrations and the presence of electron diffusion. Such an Ag^0 species may be either a real metal atom or, most likely, a trapped electron that is localized near a silver ion, without fully belonging to it but instead being shared between surroundings. In relationship to the creation of free electrons, positively-charged holes are either directly produced from the ionization of silver ions Ag^+ or trapped by these ions during the Ag^0 formation process. The trap formation globally corresponds to the mechanism: $h^+ + Ag^+ \rightarrow Ag^{2+}$. Such traps are considered to have no mobility. Additional recombination processes ($e^- + h^+$, $h^+ + Ag^0 \rightarrow Ag^+$, $e^- + Ag^{2+} \rightarrow Ag^+$) are also in competition with the charge trapping associated to the formation of the Ag^{2+} and Ag^0 species. The reaction $e^- + Ag^+ \rightarrow Ag^0$ terminates when the concentration of electrons vanishes. The resulting Ag^0 distribution qualitatively corresponds to the slightly diffused distribution of previously existing free electrons, such diffusion both resulting from the free electron diffusion itself and/or from that of the induced Ag^0 species. Correlatively, the laser-induced energy deposition is associated to a local temperature distribution (the relevance of the role of thermally activated processes will further be detailed in **Section III-3**). Still, the radial diffusion of the Ag^0 species, locally activated by the temperature distribution allows this species to take part into the following kinetic reaction: $Ag^0 + Ag^+ \rightarrow Ag_2^+$. Please note that such a thermal activation occurs despite the fact that the induced temperatures remains well below the melting temperature and glass transition temperature of the material. This first stage of silver cluster formation, initiated with the creation of Ag_2^+ species, stops either if the local concentration of the precursors Ag^0 vanishes or if its associated mobility drops down, leading to fixed Ag^0 species (as corroborated by the analysis of spatially-resolved transmission microscopy of laser-irradiated silver-containing glasses [30]). The Ag_2^+ distribution therefore qualitatively corresponds to the slightly diffused distribution of the silver cluster precursors Ag^0. Alternatively, a pair Ag^+--Ag^+ of two closely neighboring Ag^+ ions may also easily trap a free electron, directly leading to the formation of Ag_2^+ species thanks to the mechanism : Ag^+--$Ag^+ + e^- \rightarrow Ag_2^+$. Further growth of larger silver clusters follows similar photo-activated chemical pathways. By also introducing a laser-activated mobility of the Ag^+ ions, the production of silver clusters globally results from a series of reactions, corresponding generally to $x.Ag^+$ +

$y.Ag^0 \rightarrow Ag_m^{x+}$ with the nuclearity $m = x + y$ [31]. In addition to cluster growth, charge compensation mechanisms can occur between the induced clusters and surrounding reducing agents (such as non-bridging oxygen elements or other defects), leading to specific stable Ag_m^{x+} clusters with adapted nuclearities m and associated charges x^+ [30, 71, 72]. Silver clusters Ag_m^{x+} are expected to show no mobility since their diffusion and site hopping are inhibited by stearic issues. Finally, correlatively to the creation of photo-electrons, existing silver clusters located on the on-axis region of the focused laser beam are, when irradiance is high enough, photo-dissociated. As a consequence, the net budget of silver clusters formation after one single laser pulse is the balance between the photo-dissociation of pre-existing silver clusters and the photo-activated diffusion and chemical reactions of small silver elements (Ag^0 and Ag^+) to create silver clusters.

III-3. Many-pulses interaction regime and cumulative effects

Because of fast trapping processes and associated kinetic reactions, the concentrations of free electrons, holes, and intermediate component Ag^0 vanish before the next pulse, even in the case of lasers with high repetition rates of up to 100 MHz, typically. The involved processes described in **Section III-2** repeat from pulse to pulse, leading (i) to the systematic destruction of silver clusters in the intense on-axis region of the laser beam, (ii) to the pulse-after-pulse creation of photo-electrons that activate the net migration of silver elements from the on-axis region to the periphery of laser beam which corresponds to the partial consumption of the local reservoir of the available silver ions, (iii) to the progressive creation and growth of large silver clusters located at increasing radii around the periphery of the laser beam (Fig. 6). Such accumulated pulse-after-pulse processes finally lead to a cylinder-shaped distribution of fluorescent silver clusters centered on the on-axis laser beam pathway (in the case of an irradiation at fixed position). Correlatively, the described diffusion and net migration of charged species is accompanied by the creation of a non-zero space charge separation, which results in a perennial buried static electric field, locally breaking the centro-symmetry. These aspects may also involve non-trivial but possible charge compensation mechanisms involving the glass network [73 – 76].

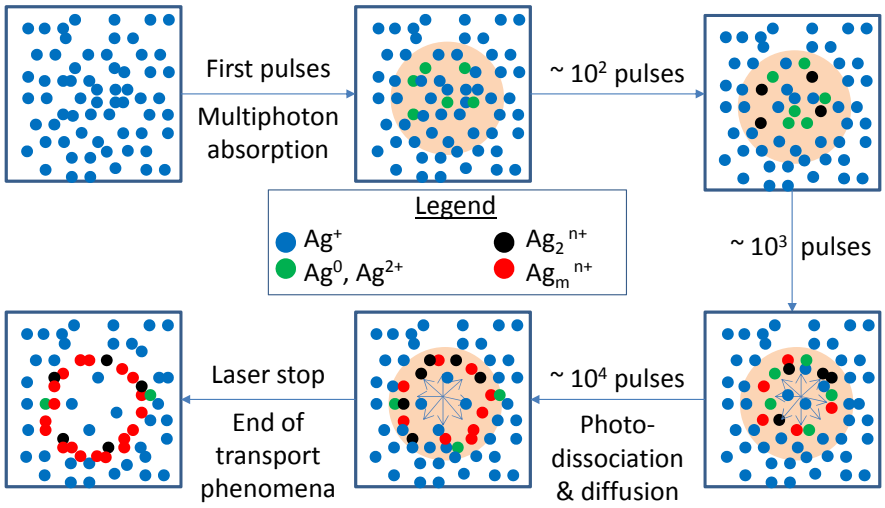

Figure 6. Physical processes involved in the pulse-after-pulse formation of silver clusters and associated nanostructures.

III-4. Multi-scale phenomenological numerical model

Most of the involved mechanisms mentioned above have been included in a phenomenological multi-scale numerical model that takes into account the pulse-to-pulse coupled equations for the energy deposition processes, the evolution of temperature T, the electron and hole concentrations n_e and n_h, and the distinct concentrations of the silver-based metal species n_M during the cumulative process of cluster formation. Because smaller clusters Ag_2^+ are not mobile species, but also because of computing time reasons, M species

are restricted to Ag^+, Ag^0, Ag^{2+} and Ag_2^+, which reasonably depicts the overall pulse-to-pulse process without altering the underlying physics by simplifying the problem. Larger clusters will thus not be considered. Other cationic elements of the glass matrix are considered as fixed elements [77], which is relevant in gallium-containing zinc phosphate matrices for temperature below the glass transition temperature T_g. Further numerical developments could include, whenever needed, the co-mobility of other elements especially like sodium ions [78]. Here, the general form of coupled equations of the derived model can be expressed as:

$$\frac{\partial T}{\partial t} = \Gamma_{D_{th}} + S_{th} \tag{1}$$

$$\frac{\partial n_e}{\partial t} = \Gamma_D\left(T, n_e\right) + \Gamma_M\left(T, n_e, \vec{E}_{dc}\right) + \Gamma_K\left(n_e, n_h, n_M\right) + \Gamma_I + \Gamma_{Diss}\left(n_M\right) \tag{2}$$

$$\frac{\partial n_h}{\partial t} = \Gamma_K\left(n_h, n_e, n_M\right) + \Gamma_I \tag{3}$$

$$\frac{\partial n_M}{\partial t} = \Gamma_D\left(T, n_M\right) + \Gamma_M\left(T, n_M, \vec{E}_{dc}\right) + \Gamma_K\left(n_M, n_h, n_e\right) \pm \Gamma_{Diss}\left(n_M\right) \tag{4}$$

$$\nabla \vec{E}_{dc} = \frac{Q\left(n_M, n_h, n_e\right)}{\varepsilon_0 \varepsilon_r} \tag{5}$$

where ε_0 and ε_{dc} are vacuum and relative permittivities. Γ_{Dth} and S_{th} in Eq. (1) are the heat diffusion term and the laser-induced heat source term, respectively. In Eqs. (2) and (4), $\Gamma_D(T, n)$ and $\Gamma_M(T, n, E_{dc})$ represent the diffusion and the mobility terms of the involved components. The hole mobility and diffusion is neglected as it is generally much lower than the electron mobility in dielectric media [79, 80]. Γ_K includes the kinetic reactions of metallic silver-based species, and Γ_I is the laser-induced electrons and holes source term in Eqs. (2) and (3). The dissociation term Γ_{Diss} (n_M) corresponds to the phenomenological description of the dissociation pathways of the involved metallic clusters on the intense on-axis region of the laser beam. Its sign is negative if the metallic species is the dissociating cluster, and it is positive if the species is the product of the dissociation. In Eq. (5), Q is the self-induced electric charge redistribution, and E_{dc} describes the associated static electric field that builds up from pulse to pulse. During the evolution of the concentrations of the involved silver-based species n_M, both the total number of silver elements and the total electrical charge are conserved. Accordingly, the main population equations of the metallic species concentrations n_M described by Eq. (4) write as:

$$\frac{\partial n_{Ag^+}}{\partial t} = \Gamma_D\left(T, n_{Ag^+}\right) + \Gamma_M\left(T, n_{Ag^+}\right) + \Gamma_K\left(n_{Ag^+}, n_e, n_h, n_{Ag^0}, n_{Ag^{2+}}, n_{Ag_2^+}\right) + \Gamma_{Diss}\left(n_{Ag_2^+}\right), \tag{6}$$

$$\frac{\partial n_{Ag^0}}{\partial t} = \Gamma_D\left(T, n_{Ag^0}\right) + \Gamma_K\left(n_{Ag^0}, n_e, n_h, n_{Ag^+}, n_{Ag^{2+}}, n_{Ag_2^+}\right), \tag{7}$$

$$\frac{\partial n_{Ag^{2+}}}{\partial t} = \Gamma_K\left(n_{Ag^{2+}}, n_e, n_h, n_{Ag^+}, n_{Ag^0}\right), \tag{8}$$

$$\frac{\partial n_{Ag_2^+}}{\partial t} = \Gamma_K\left(n_{Ag_2^+}, n_{Ag^+}, n_{Ag^0}\right) - \Gamma_{Diss}\left(n_{Ag_2^+}\right). \tag{9}$$

Energy deposition

The whole mechanism is initiated by the partial absorption of the laser pulse energy [68, 81–85], where the laser-induced electron and hole source terms for each single pulse in Eqs. (1) and (2) is:

$$\Gamma_I = \sigma_K \left(\frac{I}{\hbar\omega}\right)^K \left(n_{at}^0 - n_e\right) + \sigma \frac{I}{U_g} n_e - \frac{n_e}{\tau_r}, \tag{10}$$

where I (r, t, z) is the intensity distribution of the laser pulse. The first term corresponds to multi-photon ionization process. The second term corresponds to the impact ionization process, where σ is the inverse

Bremsstrahlung cross section, and the last term in Eq. (**10**) corresponds to the recombination process with the electron-hole recombination time τ_r. The intensity of the laser pulse decreases according to the equation:

$$\frac{\partial I}{\partial \zeta} = -\sigma_K \left(\frac{I}{\hbar\omega} \right)^K \left(n_{at}^0 - n_e \right) K\hbar\omega - \sigma I n_e, \tag{11}$$

where the input laser pulse intensity distribution shows both time and radial dependence, the time in the frame moving (with group velocity v_g of the laser pulse) is $\tau = t - z/v_g$, and the position of the laser pulse in space, correspondingly to its central time slice ($\tau = 0$) is $\zeta = v_g t$. The band-gap of the phosphate matrix is typically 5 eV, while the introduction of silver ions shifts this value around 4 eV. Energy deposition directly based on Ag^+ ionization typically deals with four-photon absorption, with the experimentally estimated cross section $\sigma_4 = 14.1 \times 10^{-118}$ $cm^8.s^3$, a value that rather matches the Keldysh's prediction for the considered irradiation parameters [**31**]. The typical initial homogeneous density of silver elements is $n^0_{at} = 7.42 \times 10^{22}$ cm^{-3} [**31**]. The experimentally measured absorption of such an ionized phosphate glass does not exceed 0.5% of the incident laser pulse energy for pulse intensities up to 8 TW/cm^2. The corresponding estimation of the free-electron density is based on the absorption measurements and appears to be of the order of 10^{17} cm^{-3}. Such small values of absorption and electron density indicate that impact ionization and subsequent electron avalanche can be neglected, which is also in agreement with the absence of dielectric breakdown in the considered laser-matter interaction process. The recombination time τ_r was adjusted around 200 femtosecond to account for both the observed electron density and absorption, by solving Eqs. (**10**) and (**11**) during the propagation of the strongly focused laser pulse in the glass along the Rayleigh length.

For a pulse train, the electron and hole source term is activated for each of the N_p pulses, each pulse being delayed by the duration $t_L = 1/f_{rep}$ with f_{rep} the repetition rate of the laser source. In the relevant irradiation parameters to activate the photo-induced silver-based reactivity under strong focusing without material damage, nonlinear effects as Kerr self-focusing and plasma-induced defocusing play no role, so that the incident laser can be considered to propagate in the same medium pulse-after-pulse, except that energy deposition differs due to the induced radial redistribution of the silver elements and induced silver-based species.

Diffusion processes

Temperature diffusion in space and time derives from:

$$\frac{\partial T}{\partial t} = D_{th}\Delta T + \frac{1}{C_p \rho} \sum_{m=1}^{N_p} S(r)\,\delta(t - m t_L), \tag{12}$$

where the heat source term S results from the local energy density deposited by each of the N_p pulses, C_p and ρ are the specific heat capacity and glass density. The heat diffusion coefficient D_{th} in the glass is assumed to be constant as the glass temperature does not exceed the glass phase transition temperature. The right-hand terms respectively account for the temperature diffusion Γ_{Dth} and the laser energy absorption S_{th} in Eq. (**1**). Diffusion Γ_D and mobility Γ_M terms of silver ions Ag^+ and electrons e^- are coupled:

$$\Gamma_D + \Gamma_M = \nabla\left(D\vec{\nabla} n \right) - \nabla\left(\mu \vec{E}_{dc} n \right), \tag{13}$$

where D is the diffusion coefficient of the considered species (namely e^-, Ag^+ and Ag^0) and n is its associated concentration, and $\mu = (q/k_B T) D$ is the mobility in the electric field E_{dc} defined according to the Einstein relation with k_B the Boltzmann constant and q the particle charge. For metallic species, the diffusion process depends on the lattice temperature T, which is thermodynamically defined after each pulse prior to any ion migration, as schemed in Fig. 6. To include thermally activated processes, the diffusion coefficient D can be expressed accordingly to a Boltzmann activation law $D(T) = D(T_0) e^{E_a/T_0} e^{-E_a/T}$, with an energy activation E_a = 0.8 eV.

Kinetic reactions

First stages of kinetic reactions to create silver clusters involve the creation and trapping of electrons and holes, and their interaction with the smaller silver species Ag^+, Ag^0, Ag^{2+} and Ag_2^+. An additional kinetic reaction depicts the phenomenology of indirect electron-hole recombination $Ag^{2+} + Ag^0 \rightarrow 2Ag^+$. In this framework, dominant kinetic reactions for holes, electrons and silver species with low nuclearity ($m \leq 2$) write:

$$\Gamma_K\left(n_e,...\right) = -K_r n_e n_h - K_r n_{Ag^{2+}} n_e - K_{Ag^0} n_{Ag^+} n_e, \tag{14}$$

$$\Gamma_K\left(n_h,...\right) = -K_r n_e n_h - K_r n_{Ag^0} n_h - K_{Ag^{2+}} n_{Ag^+} n_h. \tag{15}$$

As introduced by Eqs. (**6**) to (**9**), the kinetic reactivity of silver species writes:

$$\begin{aligned}\Gamma_K\left(n_{Ag^+},...\right) = &-K_{Ag^0} n_{Ag^+} n_e - K_{Ag^{2+}} n_{Ag^+} n_h - K_{Ag_2^+} n_{Ag^+} n_{Ag^0} \\ &+K_r n_{Ag^0} n_h + K_r n_{Ag^{2+}} n_e + 2K_{Ag^+} n_{Ag^{2+}} n_{Ag^0},\end{aligned} \tag{16}$$

$$\Gamma_K\left(n_{Ag^0},...\right) = K_{Ag^0} n_{Ag^+} n_e - K_{Ag_2^+} n_{Ag^+} n_{Ag^0} - K_r n_{Ag^0} n_h - K_{Ag^+} n_{Ag^{2+}} n_{Ag^0}, \tag{17}$$

$$\Gamma_K\left(n_{Ag^{2+}},...\right) = K_{Ag^{2+}} n_{Ag^+} n_h - K_r n_{Ag^{2+}} n_e - K_{Ag_2^+} n_{Ag^{2+}} n_{Ag^0}, \tag{18}$$

$$\Gamma_K\left(n_{Ag_2^+},...\right) = K_{Ag_2^+} n_{Ag^+} n_{Ag^0}. \tag{19}$$

The thermal dependences of kinetic constants that differ from recombination processes are separately evaluated according to the Arrhenius equation $K_{Ag}\left(T\right) = K_{Ag}\left(T_0\right)\sqrt{T/T_0}e^{E_a/T_0}e^{-E_a/T}$, with $K_{Ag}{}^+$, $K_{Ag}{}^{2+}$, $K_{Ag2}{}^+$ and , $K_{Ag}{}^0$ [**66**]. Finally, a "step-like" function centered on the laser beam axis provides the phenomenological description of the silver cluster photo-dissociation $Ag_2^+ \rightarrow Ag^+ + Ag^+ + e^-$, whose arbitrary radial profil and associated efficiency are adapteded to match experimental distributions of fluorescent silver clusters [**66**, **86**].

III-5. Reduction-oxidation potentials

In the present description and associated modeling, the glass matrix only behaves as a passive host matrix to support the spatial distributions of silver elements and associated silver species. This specifically makes sense for sufficient silver-containing concentrations (a few molar. % in phosphate glasses, typically), so that the laser-induced production of free electrons is dominantly originating from silver ions, and not from the glass matrix itself which contains defects and impurities. Yet, such modeling does not take into account any possible pulse-to-pulse cumulative modifications of the redox potential of the glass matrix itself, nor its associated spatial distribution. In other words, kinetic constants that govern the chemical reactivity of silver species are considered as truly constant during the irradiation process. This is certainly not perfectly exact, and it appears as an extremely difficult aspect to address numerically. Indeed, femtosecond laser irradiation leads to such a transient out-of-equilibrium state of the glass at the voxel that significant charge trapping occurs after a very moderate number of pulses (typically 100 pulses for an irradiation with a repetition rate at 10 MHz [**39**, **40**, **67**]). The charge stabilization leads to the creation of a buried perennial intense electric field of $10^{8\text{-}9}$ V/m, which almost corresponds to the electrical breakdown threshold of the glass. The magnitude of such an electric field $\vec{E}_{dc}\left(\vec{r}\right)$ saturates almost immediately after typically 100 pulses, as clearly observed by electric field induced second harmonic generation, which allows in turn for a local modification of the electric potential $V\left(\vec{r}\right)$ thanks to the relation $\vec{E}_{dc}\left(\vec{r}\right) = -\vec{\nabla}V\left(\vec{r}\right)$. This is considered to directly affect the local redox potential, and thus all the kinetic reactions and chemical reactivity. The growth of silver clusters significantly occurs typically after 1000 pulses, which is an order on magnitude later than what is needed to stabilized the buried static electric field. This is clearly evidenced by the cumulative dynamics of both fluorescence and third harmonic generation attribution to silver clusters [**39**, **40**, **67**]. It is remarkable indeed to note that silver clusters are being produced and stabilized exactly where the local redox potential

modification allows for a more reductive behavior, favoring the evolution of the chemical equilibrium towards larger silver species [39]. As a partial conclusion, the creation of larger silver species depends not only on mobility issues, but also on thermodynamical aspects taking into account the relative values of redox potentials of coupled silver species compared to the local glass matrix redox potential. Furthermore, one should note that only a fraction of the initial silver reservoir is truly available for the production of silver clusters, as evidenced by silver redistribution after laser irradiation ([96]). Indeed, such redox reactions imply mechanism of charge compensation that the glass matrix could not support if all the silver ions were involved.

IV - Femtosecond laser interaction in silver-containing glasses: Applications

The preparation of silver-containing oxide glasses and its subsequent femtosecond laser irradiation has locally led to remarkable linear (fluorescence and plasmonics) and nonlinear (SHG, THG) optical properties [20, 21, 30, 39, 40, 66, 67], requiring a whole description in terms of physico-chemical processes detailed in **Section III**. However, it is always difficult to jump over the gap between the laser-induced creation of local properties and the valuable demonstration of functionalities with real applicative potential. Still, such breakthroughs can be achieved by means of different approaches. *First*, functionality can result from the independent juxtaposition of material modifications with 0D dimensionality, as illustrated in **Section IV-1** with the proposed approach of high-density three-dimensional perennial optical data storage. *Second*, functionality can result from continuous modifications over long distances with 1D dimensionality, as shown in **Section IV-2** with the inscription of a new type of waveguides in bulk or fiber glasses. *Third*, functionality can be addressed by patterning 2D dimensionality, in the bulk or even directly at the glass surface as shown in **Section IV-3** with innovative surface preparation and associated reactivity. *Fourth*, functionality can result from the tailoring of electromagnetic properties, by creating an effective artificial medium with a crystal-like multi-scale lattice of sub-wavelength modifications, globally showing a true 3D dimensionality, as shown in **Section IV-3**. As a consequence, DLW techniques can modify the size, the shape, and the arrangement of the metal clusters and the whole spectrum of optical properties, which is a powerful and flexible tool to control and optimize material modifications and associated applications.

IV-1 High-density multilevel optical data storage

To overcome the storage capacity limitation, the next generation of optical recording media should be 3D, in order to increase significantly the data density. Different 3D writing and reading techniques have been proposed, including multiphoton [87] or confocal [88] configurations. Advanced approaches have even proposed strategies with a larger dimension number, up to 5D data storage [61, 89, 90]. In a different approach Royon *et al.* demonstrated that silver-containing zinc-phosphate glasses is an ideal candidate for perennial 3D optical recording as they exhibit the high stability and durability of a glass combined with the intense fluorescence of silver clusters after femtosecond laser irradiation [38] (similar to Fig. 7).

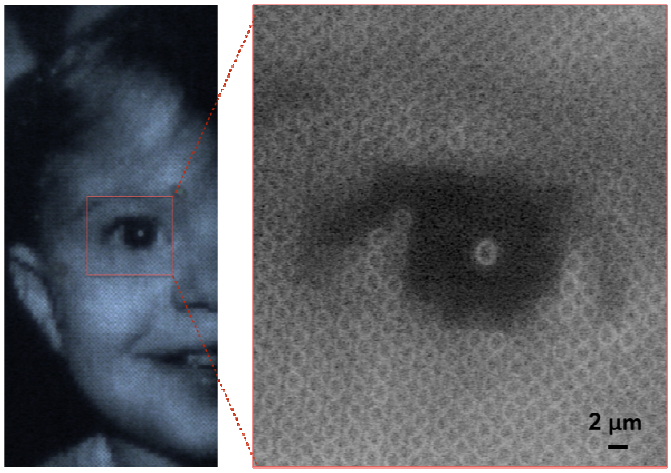

Figure 7. Optical data storage of a selected 200×200 image encoded on 256 gray levels (not shown here): (left) encoded image as a 200×200 pixels image on 256 gray levels of fluorescence emission under UV excitation ($\lambda_{exc.}$ = 365 nm), being partially recorded by wide-field fluorescence microscopy (objective 50×, NA = 0.75); (right) zoom of a region of interest. The pixels consist of fluorescent rings with 1.6 µm diameters and 7 µm depth, equally positioned in a square lattice with 2 µm spacing.

The fluorescence intensity of the photo-induced clusters is controlled via the exposure conditions of the glass and can be grayscale encoded. In this framework, such an encoding approach can be claimed as a 4D optical data storage, with 3D spatial degrees of freedom and 1D degree of freedom accounting for multi-level grey-scale fluorescence emission. This medium presents all the advantages needed for 3D optical data storage: commercial availability of the driver (Blu-ray for example), high storage capacity (possibly up to hundreds of Tbit.cm^{-3}), no photobleaching of the fluorescence, no cross-talk, and high reading speed (500 Mbit.s^{-1}). Furthermore, the temperature, ageing, and humidity tolerance of this recording medium make it suitable for perennial storage over many centuries.

Multi-dimensionnal optical data storage (in more than 3D) may have a promising future, by combining several approaches. Indeed, it would be of high interest to exploit the fluorescence dynamics due to the creation of silver clusters and form birefringence that results from the formation of nanogratings. Indeed, pioneer works have shown that surface nanogratings in silver-containing phosphate glasses can sustain silver cluster fluorescence but also nonlinear behavior with second-harmonic generation [**52**, **91**]. Further recent demonstrations have shown the concomitant existence of fluorescent silver species, silver plasmonic nanoparticles and form birefringence with phase shift and control of optical axis orientation with polarization [**92**, **93**]. Still, further research is needed to explore whether it is possible or not to control independently these distinct optical properties, which could open the route to up to 6D optical data storage.

IV-2 Light guiding in bulk and fibers, silver-sustained waveguides towards photonics circuits

In silver-containing zinc phosphate glass, DLW proceeds via the formation of silver clusters at the periphery of the interaction voxel. Abou Khalil *et al.* have shown that it allows for the production of a novel type of refractive index modification and consequently for the inscription of a new type of optical waveguides [**94**]. Here index change is not based on a standard index modification of the glass matrix itself, due to laser-induced modifications of the local density, as it is the case for *Type I*. Instead, the produced Δn is based on the localized laser-induced creation of new chemical silver species with enlarged molecular electric polarizability, locally leading to an increase of the electric susceptibility and associated refraction index change. These considerations allow for classifying this silver-supported index change as a new type of refractive index change, being independent from index modification of the glass matrix itself. Indeed, the absence of laser-induced modifications in a same non-silver-containing glass matrix ensures (i) that the corresponding ranges of irradiance and number of pulses do not affect the glass matrix itself and (ii) that the laser-matter energy deposition occurs through multi-photon ionization of the silver ions. Therefore, the

formation of silver clusters occurs for pulse energies much lower than the onset of the *Type I* modification in this glass. The involved DLW process corresponds to an extrinsic laser structuring since it mostly preserves the glass matrix while acting on the incorporated silver ions. In this framework, we labeled ***Type A*** (with *A* referring to *Argentum*) such a novel type of index modification and related waveguides sustained by the photo-induced chemistry of silver species. Such an index modification based of the laser-induced silver chemistry fully differs from the material modifications labeled *Type I*, *Type II* or *Type III*, respectively associated to isotropic index changes, to anisotropic index changes or to the creation of voids.

This novel type of positive refractive index change is compatible with waveguiding applications. As an illustration, a centimeter-long waveguide was written inside a bulk glass, exhibiting an index change $\Delta n = 2.5 \times 10^{-3}$, a single mode profile supported by each of the two silver clusters traces and showing an upper limit of propagation losses of 1.2 dB/cm [94]. Moving a step forward to the creation of an optical component such as 3D integrated circuits, a 50-50 Y-shaped beam splitter (Fig. 8) was inscribed 160 µm below the surface of a silver-containing zinc phosphate glass sample (4% molar of Ag_2O), by sequentially writing two partially overlapping S-bended waveguides. The optical component divides the input light power equally through each of the two output branches (Fig. 8a). Fluorescence image of the written beam splitter is shown in Fig. 8b. During to laser injection in the beam splitter, the output facet of the sample was imaged in two identical spots (Fig. 8c), indicating that the input beam was split into two different output branches. The near-field intensity profile shows that the transmitted power is equal in both branches within an error margin of 3.5% (Fig. 8d) confirming the inscription of a 50-50 beam splitter.

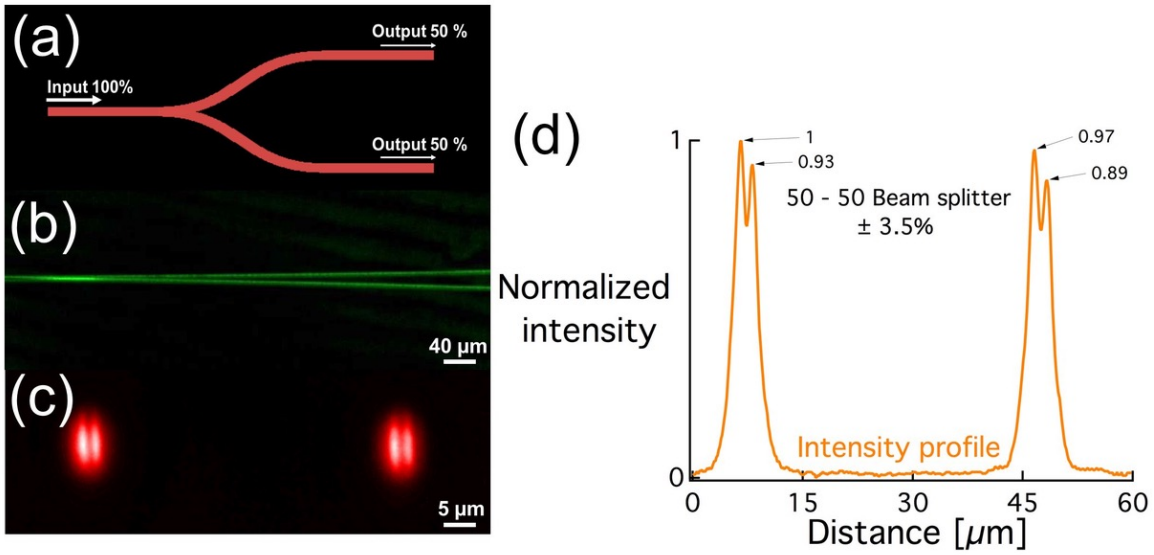

Figure 8. **(a)** Schematic presentation of a 50–50 beam splitter (top view), (**b**) fluorescent image (top view) of the written 50–50 beam splitter under 488 nm excitation and emission in the visible range, (**c**) output modes of the beam splitter, and (**d**) normalized intensity profile of the output modes. DLW conditions: 9 TW/cm^2–60 µm/s (Figure courtesy [94]).

Tailored silver-containing zinc-phosphate glasses possess excellent thermo-viscous ability and optical properties. The waveguiding properties observed in the bulk of such silver-containing glass samples were further transposed to ribbon shaped fibers made of the same material [95]. Strategy relies on the direct, homothetic drawing of rectangular silver-containing zinc-phosphate glass preforms into flat-substrate, sharp corner-edges tens-of-meters-long ribbon fibers (Fig. 9a). A ribbon fiber sample was truncated and exposed to femtosecond laser irradiation (Fig. 9b). DLW was performed typically 50 µm below the surface by linearly moving the fiber sample at controlled speeds along its longitudinal axis. Motifs were made of multiple series of lines parallel and perpendicular to the fiber main axis.

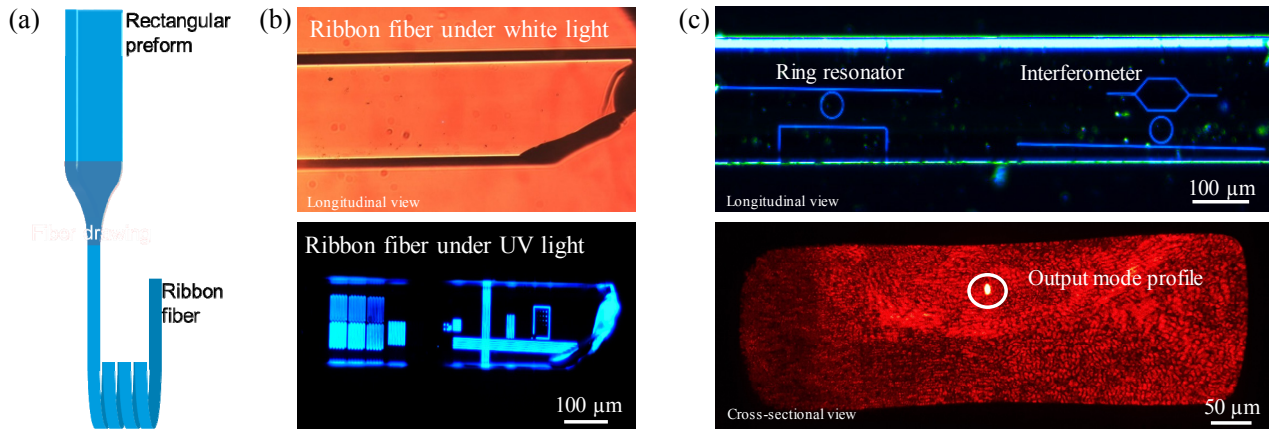

Figure 9. (a) Schematic of the thermal drawing of silver-containing zinc-phosphate glass into ribbon fibers (b) Glass fiber sample before (top) and after irradiation (bottom, under blue light $\lambda_{exc.}$ = 405 nm) (c) Schematic of ring resonators and Mach-Zehnder interferometer written in silver-containing zinc-phosphate glass ribbon fibers ($\lambda_{exc.}$ = 405 nm) (top) and output guided mode profile on fiber cross-section (bottom) [95]).

To illustrate the potential of the *in-fiber* laser-structuring method, complex light-manipulating architectures were schematically written directly in silver containing phosphate glass ribbon fibers (Fig. 9c). The first structure (top, left-side) consists in a closed resonator ring side-coupled to two light input/output bus waveguides, one of which being addressed from the side of the fiber. Alternatively (top, right-side) a Mach–Zehnder interferometer made of two arms split from a single source is coupled to one side of the resonator ring. The output mode profile of a waveguide at the end facet of a ribbon fiber is shown in the lower panel of Fig. 9c. Upon further development, this method could provide unique opportunities for applications in nonlinear optics, cavity-enhanced remote spectroscopic sensing, filtering or fully-integrated tunable photonics, as long as curvature losses are properly managed.

IV-3 Multi-scale material structuring: from 2D to 3D

The combination of DLW and chemical etching has been also developed in order to design innovative surface topology and bulk micro-channels. Such phenomena combine photo-chemistry, imprinted stress, and selective surface reaction. Sample translation along or perpendicular to the direction of the beam propagation led to the permanent formation of fluorescent structures, either corresponding to a tubular shape or to two parallel planes at the vicinity of the interaction voxel, respectively. These optical features are related to significant modifications of the local material chemistry. Thanks to such material structuring, surface engineering has been also demonstrated. Selective surface chemical etching of the glass has been obtained subsequently to laser irradiation at the location of the photo-produced structures, revealing features with nanometric depth profiles and radial dimensions strongly related to the spatial distributions of the silver clusters (Figure 10a) [96]. The cross profile of such topologies illustrates that it is possible to have an accurate control on the design of patterns at the glass surface, although such irradiation is more critical than in the bulk of the glass (due to the critical positioning exactly at the interface while considering large areas, but also due to a lower surface damage threshold than that of the bulk). Indeed, the revealed topology after etching shows spaces of 2.00±0.14 µm between two peaks, a groove width of 0.75±0.06 µm in the center of the laser interaction zone and 1.00±0.24 µm between two traces. Considering a baseline at the level of the pristine zone, the peaks represent a positive topology of 36.4±7 nm, the groove depth is -22.9±13.2nm in the center of the laser interaction zone and +10.3±9.7 nm between two laser traces. Such innovative approach may further be exploited so as to produce 2D photonics structures such as Fresnel-type lenses, arrays of antennae or effectively artificial media if smaller lateral dimensions could be achieved.

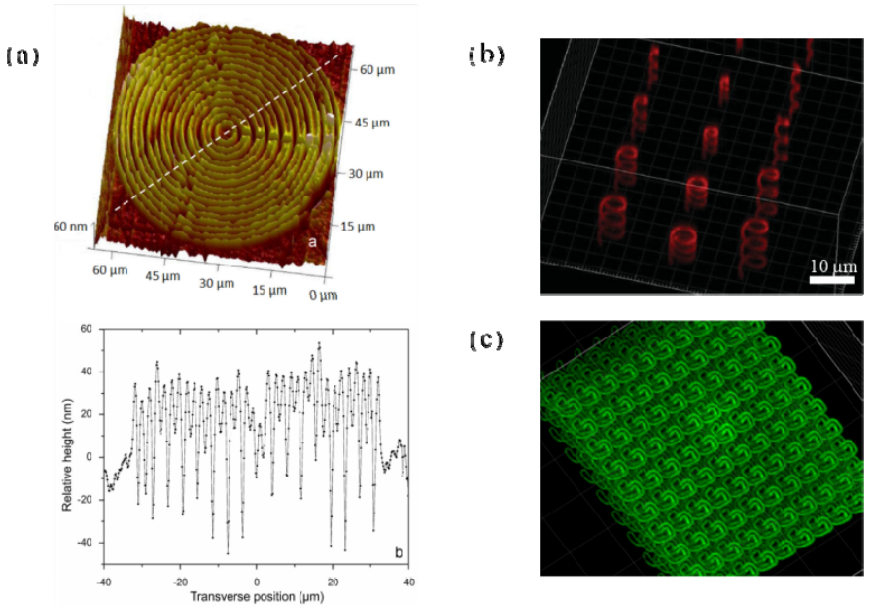

Figure 10. Laser-induced 2D and 3D structuring in silver-containing zinc-phosphate glass: (a) surface-induced structure by combining DLW and deionized water etching and its topology profile along the white dashed line (Figure courtesy [96]); (b) reconstructed confocal fluorescence microscopy image (100×, $\lambda_{exc.}$ = 405 nm) from 3D laser-induced helicoidally-distributed emitting Ag α silver clusters (Figure courtesy [**30**]); (c) bottom multi-scale blue/green emitting fluorescent pattern in glass.

Beyond the localized irradiation of independent 3D-distributed material modifications, femtosecond laser structuring can truly address the 3D multi-scale architectures. Indeed, individual local modifications can be designed with a tunable 3D shape, as shown in Fig. 10b, with oriented helicoidally-shaped distributions of silver clusters. Both helix radii and steps can be adjusted, with associated dimensions down to the micron scale while the double-line silver distribution inherently shows single-wall lateral widths of a few hundreds of nanometers. In this case, such oriented structures bear the whole panel of optical properties depicted all along this review article (namely fluorescence, nonlinear optical properties, effective Maxwell-Garnet plasmonic medium, refractive index modifications). To go further towards the laser-based production of artificial materials with tailored electromagnetic properties, it is required to fabricate a periodic lattice of locally-oriented structures, showing sub-lambda features (typically λ/10) to generate an effective medium. In this framework, we fabricated a 2D square lattice (lateral dimension 3.5 µm, typically), with the unit bearing an oriented helicoidal structure located at the points of the corresponding Bravais lattice, as shown in Fig. 10c. The global multi-scale architecture was composed of 10×10 identical helices, which opens the route for the fabrication of artificial matter in prepared glasses with much better perennial behavior than that of polymer based metamaterials for integrated photonics [**97**]. With the involved features, any possible effective behavior would be in the mid-IR spectral range, which can be compatible with the range that contains the spectral fingerprints of molecules. Still, such addressed spectral range by means of artificial meso-scale modifications has to be compatible with the transmission of the considered glass matrix, which is highly critical for oxide glasses and thus will motivate further prepared material developments.

V - Discussion

Although laser-induced glass processing has led to huge progress and applicative demonstrations these two last decades, there is still a lot of potential innovation to achieve by specifically preparing materials. Such approach of prepared materials to allow for original laser/glass interaction processes and associated properties is exactly the followed research path with silver-containing glasses. The understanding of the influence of the considered glass matrix is of prime importance to further optimize the laser/matter interaction and induced modifications in specifically-prepared glasses. In particular, it influences how silver species are stabilized in the glass, prior and post laser irradiation processes, and thus what sensitivity is possible under femtosecond laser irradiation.

For some relevant glass matrices, upon performing their synthesis with the required hand-on expertise, the insertion of silver oxide can lead to the complete dissolution of silver ions. This significant solubility of silver ions in the glass matrix is concomitant to an authorized redox stability of such silver ions, which corresponds to a sufficiently low redox potential of the glass matrix. In such situations, such as for zinc phosphate glasses, one can introduced from 0.4% up to 16% mol of Ag_2O (see Fig. 2) [**20**, **21**, **30**, **31**, **98**, **99**]. Silver can occupy an isolated Ag^+ site (labeled site A) for low insertion of silver oxide (below 1.5%) or progressively a Ag^+--Ag^+ pairs type of site (labeled site B) for an increasing insertion of silver oxide (above 1.5% up to 8%), as selectively discriminated by excitation and emission fluorescence spectroscopy. In this framework, despite the enhancement of silver species mobility, a thermal treatment at the glass transition temperature does not lead the glass system to evolve towards the formation of molecular silver species, nor to their reduction into plasmonic metallic nanoparticles. Due to the respective redox properties of both silver ions and the glass matrix, the glass is thermodynamically stable with respect to silver-based chemistry. Besides, femtosecond laser irradiation leads to a large amount of free charges (typically in the range of 10^{17} cm^{-3} [**20**]). Thus, the glass system reaches out-of-equilibrium conditions that allow for a significant pulse-to-pulse cumulative silver species mobility (Ag^0 and Ag^+) and to photo-induced chemistry of new silver species. In this framework, the creation of silver clusters mostly starts from the pre-existing silver ion pairing (Ag^+--Ag^+). Such an assertion is supported by the fact the Ag^+--Ag^+ dimmers (site B) strongly behave as electron trap centers, following the reaction Ag^+--$Ag^+ + e^- \rightarrow Ag_2^+$, leading thus to the first kind of stable silver molecular clusters showing the lowest possible nuclearity. This behavior is phenomenologically hidden in the multi-physics numerical modeling presented in **Section III-4**, with the effective successive reactions: $Ag^+ + e^- \rightarrow Ag^0$, followed by $Ag^0 + Ag^+ \rightarrow Ag_2^+$ [**66**, **67**]. Indeed, while considering silver-containing zinc phosphate glasses depicted in Fig. 2, compositions with low silver oxide concentrations (below cationic molar concentrations of 1.5%) only allow for the existence of isolated Ag^+ ions (site A), which has shown to lead to a very limited amount of induced fluorescent silver clusters under femtosecond laser irradiation. Correlatively, dual-color irradiation schemes, both with an infrared femtosecond laser inscription and a co-illumination with a cw UV beam has led to the partial reduction up to the total inhibition of production of fluorescent silver clusters [**98**]. Such a pioneer observation of inhibition process in a dielectric oxide glass corroborates the low stability of the preliminary elementary bricks, preventing to further grow larger and more stable silver clusters. This corresponds to an accessible electron trapping, either from Ag^0 ($Ag^0 + h\upsilon_{uv} \rightarrow Ag^+ + e^-$) or in a smaller proportion from Ag_2^+ ($Ag_2^+ + h\upsilon_{uv} \rightarrow Ag^0 + Ag^+$). Furthermore, once silver clusters are formed, they show a clear stability upon thermal treatment at low temperature (typically 100-200°C). This proves firstly that they do not correspond to low-stability color centers, and secondly that their redox potential has become higher than that of the glass matrix but also larger than that of the initially distributed silver ions (both sites A and B) [**100**]. However, a more intense thermal treatment slightly above the glass transition temperature can lead to the three-dimensional spatially-located precipitation of plasmonic silver metallic nanoparticles, with high filling factors associated to disconnected nanoparticles showing diameters of a few nanometers and inter-distances of 10-15 nm [**30**]. In this case, the thermally-activated precipitation of nanoparticles behaves as the thermal revealing of the femtosecond laser-induced latent image composed of silver cluster distributions. Thanks to correlative spatially- and spectrally-resolved micro-absorption measurements, the precipitation of silver nanoparticles is demonstrated to occur when some large-enough silver clusters have been preliminary created by femtosecond laser irradiation. Such large-enough silver clusters (labeled Ag_β, possibly Ag_4^{2+} or Ag_8^{2+} [**28**, **30**, **71**]) behave as nucleation centers that allow for the growth a few tens of silver elements to reach the metal phase. Smaller silver clusters, labeled Ag_α (possibly Ag_2^+), do lead to such growth and phase transition, and do not necessarily disappear (as shown by the persistence of some silver cluster absorption bands). However, their fluorescence cancels, which may result from fluorescence emission quenching due to the vicinity of the precipitated silver nanoparticles [**30**]. Indeed, only large-enough Ag_β silver clusters may be considered to show a sufficient redox potential increase, thermodynamically allowing for their growth in the considered glass matrix. This kind of behavior typically corresponds to silver-containing glasses as zinc phosphate (PZn:Ag [**20**, **30**]),

zinc-sodium phosphate (PZnN:Ag [95]) or sodium-gallium phosphate (GPN:Ag [52]) glasses. In such here-above described cases, sub-microns features of several hundreds of nanometers are achievable, by keeping an excellent optical quality of the laser irradiated voxel, without any large-scale thermally affected area [20, 30]. Finally, it should be noted that, in such zinc phosphate matrices that do not spontaneously lead to silver metallic nanoparticles with thermal treatment around T_g, it is still possible to achieve one-step laser-induced silver clusters creation and plasmonic nanoparticles together, without post heat treatment [101]. This requires either large-enough pulse energies or large enough silver concentrations, so as to significantly overpass the glass transition temperature during the irradiation and to locally melt the material. However, this results in large thermally-affected zones over dimensions much larger that the focused laser beam [101, 102]. Such material modifications bear also bear large stress due to the thermal expansion during irradiation, which lowers the optical quality of the irradiated area and may thus be detrimental to photonics applications requiring sub-micron features.

For silicate or germinate glass matrices, the initial solubility of silver oxide is lower. Therefore, the redox potential of the glass matrix appears higher, with respect to silver ions and small silver clusters. In this case, the glass matrix allows for the stabilized existence of some silver clusters, additionally to that of silver ions. Femtosecond laser irradiation can therefore directly lead in a single-step procedure to the local precipitation of metallic silver nanoparticles, without any thermal post-treatment [103]. For such glass matrices that favor the clustering and reduction of silver species, the thermal treatment around the glass transition temperature can directly lead to the randomly-distributed precipitation of metallic nanoparticles, which is associated to filling factors several orders of magnitude lower than that of the laser-induced creation [103]. For such glass matrices, two independent routes allow the access to effective Maxwell-Garnett-like composite metal-dielectric glassy materials, as for the silver-doped lanthanum boro-germanate (LBG:Ag) glass matrix [103]. In this framework, heavy metal oxide glass matrices with relevant optical transmission in the mid-IR spectral range (especially in the 3-5 μm range for spectroscopic applications in the fingerprint spectral region of molecules), such as barium gallogermanate glass (BGG) [104], are also expected to favor the displacement of silver chemical equilibrium towards the creation of high nuclearity species, silver clusters and subsequently plasmonic nanoparticles.

While the insertion of silver oxide has been considered during the synthesis of the glass, the sub-surface incorporation of silver ions is also a possible route, including either the ionic exchange during the glass dipping in molten silver nitrites or silver metal deposition and subsequent injection by thermal poling. The later has already led to sub-surface silver ion injection in both a borosilicate and a sodo-calcite glass matrix, leading to the localized creation of silver clusters under femtosecond laser irradiation [66]. The direct insertion of silver ions in the glass matrix at the melting step or their post-synthesis injection both allow for the femtosecond laser activated photo-chemistry of silver species with remarkable optical properties. This tends to demonstrate the universality of such an extrinsic glass modification that is mostly supported by the silver species (and not from the glass matrix itself), as long as silver elements can be incorporated to the considered glass matrix. Finally, the multi-scale engineering of the spatial distributions of extrinsic laser structuring can be addressed by tailoring the femtosecond beam shape, either with its phase or polarization distributions. Such prepared beams correspond to structured light that possibly bear optical singularities (namely optical vortices), as well as the existence of both spin and angular momenta carried by the beam. Such an engineering of the optical field distribution at the voxel allows for innovative linear and nonlinear optical patterning with structured light, giving access to modification topologies and geometries that cannot be achieved with a standard Gaussian beam [105, 106].

VI. Conclusion and perspectives

The present review proposes an extensive description and modeling of phenomena that occur during femtosecond laser structuring of silver-containing non-conventional glasses in the accumulation regime with high repetition rate irradiation. It also highlights the role of the host glassy matrix, including the influence of

its structural arrangement, the sensitivity for photo-activation of silver mobility and chemical reactivity, as well as the implied stabilization of silver species with respect to the relative redox potentials of the considered glass environment and the different types of silver species. Such complete description of the multi-physics and multi-scale (both in time and space) processes at play during laser irradiation allows for a comprehensive understanding of the global material modification that leads to remarkable optical but also physico-chemical properties. This in turns gives a meaningful insight to further develop new materials with dedicated behavior under laser irradiation, so as to master improved prepared material potentialities and to further address a broadband panel of the technological issues and associated applications.

Indeed, beyond the presented applicative achievements, femtosecond laser structuring of prepared photo-sensitive glasses has real perspectives of scientific development and industrial technological transfer. This includes the development of optical data storage with large dimensionalities (3D, and more), the exploitation of multi-scale architectures with linear and nonlinear optical properties to create original and robust integrated photonic structures as photonic crystals or artificial matter (namely 2D or 3D metamaterials). Additionally, the reported waveguiding allows for interesting perspectives, including bulk- or fiber-based sensor applications with evanescent coupling at the material surface with the environment. The local development of neighboring waveguiding and plasmonic structures may allow for promising combinations, including new schemes for surface enhanced Raman scattering (SERS). Finally, surface preparation can further lead to high selectivity by tailoring the coupling between topological modifications and the local nano-scale chemical reactivity. As a conclusion, among technological breakthroughs in photonics leading to a potential societal impact, one can be sure that many will come from a highly multi-disciplinary approach, with a high level of expertise shared between communities such as material science, laser/matter interaction, environmental sciences, biology or communication and computing sciences.

ACKNOWLEGDMENTS

This study has been carried out with financial support from the French State, managed by the French National Research Agency (ANR) in the frame of "the Investments for the future" Programme IdEx Bordeaux – LAPHIA (**ANR-10-IDEX-03-02**), as well as in the frame of the ANR program **N° ANR-17-CE08-0042-01**. This study was also supported the French Region Nouvelle Aquitaine, with the program **n° 2016 – 1R10107**. This study finally supported by the Canadian programs of Natural Sciences and Engineering Research Council (NSERC, grant **CG101779**), Canada Foundation for Innovation (CFI, grant **GF072345**), and Fonds de Recherche du Québec-Nature et Technologies (FQRNT, grants **FT097991** and **CO201310**).

References

1. A. Arriloa, S. Gross, M. Ams, T. Gretzinger, D. Le Coq, R. P. Wang, H. Ebendorff-Heidepriem, J. Sanghera, S. Bayya, Opt. Mater. Expr. 7(3), 698- 711 (2017).

2. M. Ams, G. D. Marshall, P. Dekker, J. A. Piper and M. J. Withford, Laser & Photon. **3**(6), 535–544 (2009).

3. T. Meany, M. Gräfe, R. Heilmanz, A. Perez-Leija, S. Gross, M. J. Steel, M. J. Withford, and A. Szameit, Laser Photonics Rev. **9**(4), 363–384 (2015).

4. M. Haque, K. K. C. Lee, S. Ho, L. A. Fernandes and P. R. Herman, Lab Chip **14**, 3817 (2014).

5. A. Podlipensky, A. Abdolvand, G. Seifert and H. Graener, Appl. Phys., A Mater. Sci. Process. **80**(8), 1647–1652 (2005).

6. Y. Dai, B. Zhu, J. Qiu, H. Ma, B. Lu and B. Yu, Chem. Phys. Lett. **443**(4-6), 253–257 (2007).

7. Y. Cheng, K. Sugioka, M. Masuda, K. Shihoyama, K. Toyoda and K. Midorikawa, Opt. Express **11**(15), 1809–1816 (2003).

8. M. Masuda, K. Sugioka, Y. Cheng, N. Aoki, M. Kawachi, K. Shihoyama, K. Toyoda, H. Helvajian and K. Midorikawa, Appl. Phys., A Mater. Sci. Process. **76**(5), 857–860 (2003).

9. Y. Shimotsuma, M. Sakakura, K. Miura, J. Qiu, P. G. Kazansky, K. Fujita and K. Hirao, J. Nanosci. Nanotechnol. **7**(1), 94–104 (2007).

10. K. Miura, J. Qiu, T. Mitsuyu and K. Hirao, Opt. Lett. **25**(6), 408–410 (2000).
11. A. Aki Unal, A. Stalmashonak, G. Seifert and H. Graener, Phys. Rev. B **79**, 115411 (2009)
12. A. Akin Unal, A. Stalmashonak, H. Graener and G. Seifert, Phys. Rev. **B** 80, 115415 (2009).
13. B. Hua, Y. Shimotsuma, M. Nishi, K. Miura, K. Hirao, J. Laser Micro/Nanoengineering **2**, 36–39 (2007).
14. J. Qiu, X. Jiang, C. Zhu, H. Inouye, J. Si and K. Hirao, Opt. Lett. 29(4), 370–372 (2004).
15. J. Qiu, K. Miura and K. Hirao, J. Non-Cryst. Sol. **354**, 1100–1111 (2008).
16. J. Qiu, K. Miura, T. Suzuki, T. Mitsuyu and K. Hirao, Appl. Phys. Lett. **74**(1), 10–12 (1999).
17. J. Qiu, P. G. Kazanski, J. Si, K. Miura, T. Mitsuyu, K. Hirao and A. L. Gaeta, Appl. Phys. Lett. **77**(13), 1940–1942 (2000).
18. Y. Liu, M. Shimizu, B. Zhu, Y. Dai, B. Qian, J. Qiu, Y. Shimotsuma, K. Miura and K. Hirao, Opt. Lett. **34**(2), 136–138 (2009).
19. L. Siiman, J. Lumeau and L. B. Glebov, J. Non-Cryst. Sol. **354**, 4070–4074 (2008).
20. M. Bellec, A. Royon, B. Bousquet, K. Bourhis, M. Treguer, T. Cardinal, M. Richardson and L. Canioni, Opt. Express **17**(12), 10304–10318 (2009).
21. L. Canioni, M. Bellec, A. Royon, B. Bousquet and T. Cardinal, Opt. Lett. **33**(4), 360–362 (2008).
22. S. D. Stookey, Ind. Eng. Chem. **41**(4), 856–861 (1949).
23. Y. Kondo, K. Miura, T. Suzuki, H. Inouye, T. Mitsuyu, K. Hirao, J.Non-Cryst. Sol. **253**, 143–156 (1999).
24. A. Royon, Y. Petit, G. Papon, M. Richardson and L. Canioni, Opt. Mater. Express **1**(5), 866-882 (2011). [Invited]
25. R. R. Gattass and E. Mazur, Nat. Photonics **2**(4), 219–225 (2008).
26. M. Ams, G. D. Marshall, P. Dekker, J. A. Piper and M. J. Withford, Laser Photonics Rev. **3**(6), 535–544 (2009).
27. Y.-L. Zhang, Q.-D. Chen, H. Xia and H.-B. Sun, Nano Today **5**(5), 435–448 (2010).
28. R. Espiau de Lamaestre, H. Béa, H. Bernas, J. Belloni and J. L. Marignier, Phys. Rev. B **76**, 205431 (2007).
29. M. V. Shestakov, X. Chen, W. Baekelant, A. S. Kuznetsov, V. K. Tikhomirov, J. Hofkens and V. V. Moshchalkov, RSC Adv. **4**, 20699 (2014).
30. N. Marquestaut, Y. Petit, A. Royon, P. Mounaix, T. Cardinal and L. Canioni, Adv. Funct. Mater., **24**(37), 5824-5832 (2014).
31. K. Bourhis, A. Royon, M. Bellec, J. Choi, A. Fargues, M. Treguer, J.-J. Videau, D. Talaga, M. Richardson, T. Cardinal and L. Canioni, J. Non-Cryst. Solids **356**, 2658 (2010).
32. K. Bourhis, A. Royon, G. Papon, L. Canioni, N. Makria, Y. Petit, T. Cardinal, J. Non-Cryst. Solids. **377**, 142–145 (2013).
33. N. G. Boetti, G. C. Scarpignato, J. Lousteau, D. Pugliese, L. Bastard, J-E. Broquin and D. Milanese, J. Opt. **17**, 06570 (2015).
34. J. H. Campbell and T. I. Suratwala, J. Non-Cryst. Solids, **263–264**, 318-34 (2000).
35. N. G. Boetti, D. Pugliese, E. Ceci-Ginistrelli, J. Lousteau, D. Janner, and D. Milanese, Appl. Sci. **7**, 1295 (2017).
36. R.K. Brow, J. Non-Cryst. Solids **263-264**, 1-28 (2000).
37. M. Bellec, A. Royon, K. Bourhis, J. Choi, B. Bousquet, M. Treguer, T. Cardinal, J.-J. Videau, M. Richardson and L. Canioni, J. Phys. Chem. C **114**, 15584 (2010).
38. A. Royon, K. Bourhis, M. Bellec, G. Papon, B. Bousquet, Y. Deshayes, T. Cardinal and L. Canioni, Adv. Mater. **22**, 5282–5286 (2010).
39. G. Papon, Y. Petit, N. Marquestaut, A. Royon, M. Dussauze, V. Rodriguez, T. Cardinal and L. Canioni, Opt. Mater. Express **3**, 1855 (2013).
40. G. Papon, N. Marquestaut, Y. Petit, A. Royon, M. Dussauze, V. Rodriguez, T. Cardinal and L. Canioni, J. Appl. Phys. **115**, 113103 (2014).
41. I. Belharouak, C. Parent, B. Tanguy and G. Le Flem, J. Non-Cryst. Solids **244**, 238-249 (1999).
42. I. Belharouak, F. Weill, C. Parent, G. Le Flem and B. Moine, J. Non-Cryst. Solids. **293**, 649–656 (2001).
43. A. Podlipensky, A. Abdolvand, G. Seifert and H. Graener, Appl. Phys., A Mater. Sci. Process. **80**(8), 1647–1652 (2005).

44. E. G. Bondarenko, V. O. Kabanov, G. O. Karapetyan and O. V. Yanush, J. Appl. Spectrosc. **35**(1), 744-749 (1981).
45. M. Mesnaoui, M. Maazaz, C. Parent, B. Tanguy and G. Le Flem, Eur. J. Solid State Inorg. Chem. **29**(6), 1001-1013 (1992).
46. M. Mesnaoui, C. Parent, B. Tanguy, M. Maazaz, G. Le Flem, B. Moine and C. Pedrini, Adv. Mat. Res., **1-2**, 83-88 (1994).
47. E. Borsella, F. Gonella, P. Mazzoldi, A. Quaranta, G. Battaglin and R. Pollonic, **284**, 6, 429-434 (1998).
48. I. Belharouak, E. Fargin, C. Parent and G. Le Flem, Solid State Sci. **1**(5), 287-300 (1999).
49. I. Belharouak, H. Aouad, M. Mesnaoui, M. Maazaz, C. Parent, B. Tanguy, P. Gravereau and G. Le Flem, J. of Solid **45** (1), 97-103 (1999).
50. A. Meijerink, M. Van Heek and G. Blasse, J. Phys. Chem. Solids **54**, 901–906 (1993).
51. I. Belharouak, C. Parent, P. Gravereau, J-P. Chaminade, G. Le Flem and B. Moine, J. Solid State Chem. **149**, 284-291 (2000).
52. M. Vangheluwe, F. Liang, Y. Petit, P. Hée, Y. Ledemi, S. Thomas, E. Fargin, T. Cardinal, Y. Messaddeq, L. Canioni, R. Vallée, Opt. Lett. **39**(9), 5191-5494 (2014).
53. B. Atoussi, C. Pedrini, B. Moine and C. Madej, Physics Status Solidi B **128**(2), 683-692 (1985).
54. C. B. Schaffer, A. Brodeur and E. Mazur, Measurement Science and Technology **12**, 1784-1794 (2001).
55. B. C. Stuart, M. D. Feit, S. Herman, A. M. Rubenchik, B. W. Shore and M. D. Perry, Phys. Rev. B **53**, 1749-1761 (1996).
56. S. S. Mao, F. Quéré, S. Guizard, X. Mao, R. E. Russo, G. Petite and P. Martin, Appl. Phys. A **79**, 1695-1709 (2004).
57. M. Ams, G. D. Marshall, P. Dekker, M. Dubov, V. K. Mezentsev, I. Bennion and M. J. Withford, IEEE Journal of Selected Topics in Quantum Electronics **14**, 1370-1381 (2008).
58. R. R. Gattass and E. Mazur, Nature Photonics **2**, 219-225 (2008).
59. K. Miura, J. Qiu, H. Inouye, T. Mitsuyu and K. Hirao, Appl. Phys. Lett. **71**, 3329-3331 (1997).
60. S. Juodkazis, K. Nishimura, S. Tanaka, H. Misawa, E. G. Gamaly, B. Luther-Davies, L. Hallo, P. Nicolai and V. T. Tikhonchuk, Phys. Rev. Lett. **96**, 166101 (2006).
61. Y. Shimotsuma, P. G. Kazansky, J. Qiu and K. Hirao, Phys. Rev. Lett. **91**, 247405 (2003).
62. P. P. Rajeev, M. Gertsvolf, E. Simova, C. Hnatovsky, R. S. Taylor, V. R. Bhardwaj, D. M. Rayner and P. B. Corkum, "Memory in Nonlinear Ionization of Transparent Solids," Physical Review Letters **97**, 253001 (2006).
63. F. Liang, R. Vallée, D. Gingras, and S. L. Chin, "Role of ablation and incubation processes on surface nanograting formation," Opt. Mater. Express **1**, 1244-1250 (2011).
64. F. Liang, R. Vallée, and S. L. Chin, "Mechanism of nanograting formation on the surface of fused silica," Opt. Express **20**, 4389-4396 (2012)
65. M. Bellec, A. Royon, K. Bourhis, J. Choi, B. Bousquet, M. Treguer, T. Cardinal, J.-J. Videau, M. Richardson and L. Canioni, J. Phys. Chem. C **114**, 15584-15588 (2010).
66. E. Smetanina, B. Chimier, Y. Petit, N. Varkentina, L. Hirsch, E. Fargin, T. Cardinal, L. Canioni, and G. Duchateau, Phys. Rev. A 93, 013846 (2016).
67. E. Smetanina, B. Chimier, Y. Petit, A. Royon T. Cardinal, L. Canioni, and G. Duchateau, Opt. Lett. **42**(9), 1688-1691 (2017).
68. L. V. Keldysh, Soviet Physics JETP **20**, 1307-1314 (1965).
69. L. N. Gaier, M. Lein, M. I. Stockman, G. L. Yudin, P. B. Corkum, M. Yu Ivanov and P. L. Knight, J. Modern Optics **52**, 1019-1030 (2005).
70. L. N. Gaier, M. Lein, M. I. Stockman, P. L. Knight, P. B. Corkum, M. Yu Ivanov and G. L. Yudin, J. Physics B: Atomic, Molecular and Optical Physics **37**, L57-L67 (2004).
71. B. G. Ershov, G. V. Ionova, A. A. Kiseleva, Rus. J. Phys. Chem. **69**, 239 (1995).
72. A. Simo, J. Polte, N. Pfander, U. Vainio, F. Emmerling, K. Rademann, J. Am. Chem. Soc. **134**, 18824 (2012).
73. N. Varkentina, M. Dussauze, A. Royon, M. Ramme, Y. Petit, L. Canioni, "High repetition rate femtosecond laser irradiation of fused silica studied by Raman spectroscopy," Opt. Mater. Expr. **1**(6), 79-90 (2016).

74. M. Lancry, B. Poumellec, J. Canning, K. Cook, J.-C. Poulin, and F. Brisset, Laser Photon. Rev. **3** (11), (2013).
75. K. Nakamoto, "Infrared and Raman spectra of inorganic and coordination compounds. Part B. Applications in Coordination, Organometallic, and Bioinorganic Chemistry," John Wiley & Sons Inc., Hoboken, New Jersey, USA, 6th edition (2009).
76. M. Dussauze, V. Rodriguez, A. Lipovskii, M. Petrov C. Smith, K. Richardson, T. Cardinal, E. Fargin, and E. I. Kamitsos, J. Phys. Chem. C **114**, 12754–12759 (2010).
77. S. Anvari, C. Hogarth, and G. Moridi, J. Mater. Sci. **26**, 3639 (1991).
78. M. Martin, J.-J. Videau, L. Canioni, F. Adamietz, L. Sarger, and G. Le Flem, Appl. Opt. **39**(3), 435–440 (2000).
79. N. Bulgakova, R. Stoian, A. Rosenfeld, I. Hertel, W. Marine, and E. Campbell, Appl. Phys. A **81**, 345 (2005).
80. N. M. Bulgakova, R. Stoian, A. Rosenfeld, I. V. Hertel, and E. E. B. Campbell, Phys. Rev. B **69**, 054102 (2004).
81. B. C. Stuart, M. D. Feit, S. Herman, A. M. Rubenchik, B. W. Shore, and M. D. Perry, Phys. Rev. B **53**, 1749 (1996).
82. D. Arnold and E. Cartier, Phys. Rev. B **46**, 15102 (1992).
83. D. F. Price, R. M. More, R. S. Walling, G. Guethlein, R. L. Shepherd, R. E. Stewart, and W. E. White, Phys. Rev. Lett. **75**, 252 (1995).
84. A. Couairon, L. Sudrie, M. Franco, B. Prade, and A. Mysyrowicz, Phys. Rev. B **71**, 125435 (2005).
85. J. Rolle, L. Bergé, G. Duchateau, and S. Skupin, Phys. Rev. A **90**, 023834 (2014).
86. P. Atkins and J. de Paula, *Physical Chemistry for the Life Sciences* (Oxford University Press, Oxford, UK, 2011).
87. J. H. Strickler , W. W. Webb , Opt. Lett. **16**, 1780 (1991).
88. S. Pan , A. Shih , W. Liou , M. Park , J. Bhawalkar , J. Swiatkiewicz , J. Samarabandu , P. N. Prasad , P. C. Cheng , Scanning **19**, 156 (1997).
89. J. Zhang, M. Gecevičius, M. Beresna, and P. G. Kazansky, Phys. Rev. Lett. **112**, 033901 (2014).
90. P. Zijlstra, J. W. M. Chon & M. Gu, Nature, **459**, 410-413 (2009).
91. M. Vangheluwe, Y. Petit, F. Liang, P. Hée, Y. Ledemi, S. Thomas, E. Fargin, T. Cardinal, Y. Messaddeq, L. Canioni, R. Vallée, Proc. IEEE Xplore (2015). DOI : 10.1109/PN.2015.7292520.
92. A. Lipat'ev, G. Yu. Shakhgil'dyan, T. O. Lipat'eva, S. V. Lotarev, S. S. Fedotov, M. P. Vetchinnikov, E. S. Ignat'eva, N. V. Golubev, V. N. Sigaev, and P. G. Kazanskii,, Glass and Ceramics **73**(7-8), 277-282 (2016).
93. A. S. Lipat'ev, M. P. Vetchinnikov, G. Yu. Shakhgil'dyan, S. V. Lotarev, A. M. Vasetskii, and V. N. Sigaev, Glass and Ceramics **74**(11-12), 385-388 (2018).
94. A. Abou Khalil, J-P. Bérubé, S. Danto, J-C. Desmoulin, T. Cardinal, Y. Petit, R. Vallée and L. Canioni, Sci. Rep. **7**: *11124* (2017).
95. S. Danto, F. Désévédavy, Y. Petit, J,-C. Desmoulin, A. Abou Khalil, C. Strutynski, M. Dussauze, F. Smektala, L. Canioni, T. Cardinal, Adv. Opt. Mater. **4**(1), 162-168 (2016).
96. J-C. Desmoulin, Y. Petit, L. Canioni, M. Dussauze, M. Lahaye, H. M. Gonzalez, E. Brasselet and T. Cardinal, J. Appl. Phys. **118**, 213104 (2015).
97. J. Kaschke, and M. Wegener, Optics Letters **40**(17), 3986-3989 (2015).
98. Y. Petit, K. Mishchik, N. Varkentina, N. Marquestaut, A. Royon, I. Manek-Hönninger, T. Cardinal, and L. Canioni, Opt. Lett. **40**(17), 4134-4137 (2015).
99. G. Shakhgil'dyan, A. S Lipat'ev, M. P. Vetchinnikov, V. V. Popova, S. V. Lotarev and V. N. Sigaev Glass and Ceramics **43**, 420-422 (2017).
100. A. Royon, K. Bourhis, L. Béchou, T. Cardinal, L. Canioni, Y. Deshayes, Microelectronics Reliability **53**, 1514–1518 (2013).

101. G.Yu. Shakhgildyan, A.S. Lipatiev, M.P. Vetchinnikov, V.V. Popova, S.V. Lotarev, N.V. Golubev, E.S. Ignat'eva, M.M. Presniakov, V.N. Sigaev, J. Non-Cryst. Solids **481**, 634-642 (2018).
102. M. Shimizu, M. Sakakura, M. Ohnishi, Y. Shimotsuma, T. Nakaya, K. Miura, and K. Hirao, J. Appl. Phys. **108**(7), 073533 (2010).
103. M. Vangheluwe, Y. Petit, N. Marquestaut, E. Fargin, A. Corcoran, F. Liang, R. Vallée, T. Cardinal, & L. Canioni, Opt. Mat. Express **6**(3), 742-748 (2016).
104. J.-P. Bérubé, A. Le Camus, S. Messadeq, Y. Petit, Y. Messadeq, L. Canioni, and R. Vallée, Opt. Mater. Express **7**(9), 3124-3135 (2017).
105. K. Mishchik, Y. Petit, E. Brasselet, A. Royon, T. Cardinal, and L. Canioni, Opt. Lett. **40**(2), 201-204 (2015).
106. E.-J. Lee, Y. Petit, E. Brasselet, T. Cardinal, S.-H. Park, L. Canioni, Opt. Express **25**(9), 10565-10573 (2017).